Proposal of a longitudinally pumped saturated Ni-like Mo ion x-ray laser at 18.9 nm

Ruxin Li, Tsuneyuki Ozaki, Teruto Kanai, and Hiroto Kuroda

Institute for Solid State Physics, The University of Tokyo, 7-22-1 Roppongi, Minato-Ku, Tokyo 106, Japan

(Received 1 December 1997; revised manuscript received 22 January 1998)

We reexamine the transient gain scheme in this paper and develop this scheme with a new pumping geometry for designing a compact and highly efficient Ni-like Mo ion soft-x-ray laser. Model calculations show that a saturated amplification of soft x rays at 18.9 nm can be realized by using a 1.05 μm driving laser with only several hundred millijoule energy in a picosecond pulse. We propose a longitudinally pumping geometry for the high transient gain x-ray laser, in order to improve the pumping efficiency and to overcome some limitations of the present transient gain laser. [S1063-651X(98)03806-9]

PACS number(s): 52.75.Va, 42.55.Vc

I. INTRODUCTION

A very important objective in the development of x-ray lasers is to attain a highly coherent and saturated amplified output at short wavelength from a small-scaled facility, the so-called ''table-top'' system. Considerable progress in increasing the efficiency of collisionally pumped soft-x-ray lasers and downsizing the driver has been achieved recently [1–5]. Saturation operation is desired since it means that the maximum power possible for a given volume of excited plasma can be extracted by the stimulated emission, and thus the pumping efficiency can be maximized. Gain saturation has been demonstrated in the Ne-like Zn [6], Ge [7], Se [8], Y [9], and Ni-like Ag [2] and Sm [3] ion x-ray lasers in laser-produced plasmas, with a driver energy ranging from several kJ to 0.1 kJ in pulses lasting for ~0.1 to ~1 ns. To pump the short wavelength x-ray laser, the plasma has to be excited with very high flux density; a very fast pumping is therefore very necessary in order to reduce the energy requirement. The main idea of the transient gain scheme [4,10] for the electron collisional excitation x-ray laser mechanism is to overheat the electrons in a very short (transient) time scale by using a powerful ps pulse. This leads to very high small-signal gain with short duration, and it is very attractive among several candidate approaches for a compact ''table-top'' soft-x-ray laser [11]. This scheme offers the possibility of realizing a $\triangle n > 0$ transition laser pumped by the electron collision excitation [10]. In the transient gain mode, the first optical laser pulse is usually a long laser pulse with about 1 ns duration that generates, heats, and ionizes the plasma, while the second pulse is a short pulse with several ps duration that overheats the preplasma and excites the ions to produce a very large transient population inversion through strong monopole electron collisional excitation from the ground state of Ne-like or Ni-like ions. This kind of laser, different from the traditional collisional laser that operates in the quasi-steady-state (QSS) region [2,3,5–9], operates in a very high density region near the critical surface, and the amplification is therefore very sensitive to the refraction and the driving conditions. The traveling wave pumping mode is desirable since the gain duration is usually of the order of 10 ps or even shorter. A very high gain of 19 cm^{-1} has been experimentally demonstrated in the Ne-like Ti ion laser at 32.6 nm, and the GL product was measured to be 9.5 in this recent work [4]. However, the gain-length product (GL) value is still too low for a saturated operation. This first, to our knowledge, experimental result of the transient gain scheme and several theoretical analyses, that followed indicate that considerable effort should be contributed to overcoming several disadvantages of this scheme, mainly the stability of the gain region, which is limited by the refraction and the short-lived gain, for the purpose of obtaining a large GL value.

Recently simulations have been performed for the transient gain x-ray laser in Ne-like Se [12], Ge [13,14], Ti [14], and Ni-like Mo [15] ions. As known, the Ni-like ion laser scheme has, in principle, a more favorable scaling of laser wavelength with the energy of the optical laser driver. We reexamine the transient gain scheme in this paper and develop this scheme with a new pumping geometry for designing a compact and highly efficient Ni-like ion soft-x-ray laser, specifically, the Ni-like Mo ion laser at 18.9 nm. The motivation behind the design of a Ni-like Mo ion laser is twofold. As known, the ratio of lifetimes of the upper to lower laser level is relatively small for the middle-Z ($Z = 40–50$) Ni-like ions (i.e., the ratio is 2.5 for $Z = 42$ and is 10 for $Z = 60$) [5]; it is therefore relatively difficult to get large population inversion under QSS approximation. The opacity issue plays an important role in the operation of this kind of laser. We attempt to use the transient gain scheme to overcome this limitation. The QSS Ni-like Mo laser scheme was proposed several years ago [16,17], but it has never been experimentally demonstrated, though the requirement of experimental conditions seems easy to fulfill. We reexamine this laser scheme and try to develop it with the new transient gain scheme. The second motivation behind this design is to compare the transient gain laser in Ne-like Ge and Ni-like Mo ions, to see how different the parameter space is for the Ne-like and Ni-like ion lasers operating at similar lasing wavelengths. Model calculation shows that a saturated amplification of soft-x-rays at 18.9 nm by Ni-like Mo ions can be realized by using a 1.05-μm driving laser with only several hundred mJ energy in a picosecond pulse. We propose a longitudinally pumping geometry for this high transient gain laser, in order to improve the efficiency and overcome the existing limitations. This pumping geometry has several advantages. First, the gain region can be chosen to locate spatially at a certain distance away from the critical surface so

as to avoid using the steep critical surface and to relieve the large refraction caused by the very steep density gradient, partly solving the problem of gain region stability. Second, this pumping geometry can automatically fulfill the requirement of traveling wave pumping. Third, this method can directly deposit the excitation laser energy into the desired gain volume in the order to avoid any waste of the energy deposited in the other region, which is considerable if pumping transversely, since the first pulse is usually a long pulse that produces a long scale-length preplasma and thus the nonlocal absorption of the second pulse is pronounced. However, it is difficult to obtain long effective medium length in the longitudinally pumping mode due to the transmittance and the refraction of the pumping laser beam through the high-density plasma medium. We should therefore maximize the gain coefficient so that a large enough GL value can be attained by using a medium of only several mm long.

This paper is structured in the following way. In Sec. II we describe briefly the model used in this work. In Sec. III we present the results of test calculations for the transient gain lasers in Ne-like Ge and Ni-like Mo ions, and compare them with the results obtained with two sophisticated codes [13–15], in order to check the validity of our simplified model. In Sec. IV we design a longitudinally pumped high gain Ni-like Mo ion x-ray laser at 18.9 nm. We summarize this work in the final section.

II. MODEL

The basic process of the laser plasma interaction involved in the transient gain scheme can be understood intuitively. The preplasma with an appropriate abundance of Ne-like or Ni-like ions can be effectively prepared by the laser ablation of solid targets, or alternately by a fast pulse discharge. We consider the former way in this work and the duration of the first ablating laser pulse is of the order of 1 ns. Then a powerful ps pulse arriving after an appropriate delay heats and excites the plasma quickly and produces large transient gain. Regarding this particular situation, the description of the laser plasma interaction can be divided into two separated parts. The interaction of the first ns pulse with the solid target can be treated by a steady state ablation and the corresponding hydrodynamic process can be described approximately by a self-similar expansion model. As to the interaction of the second pulse with the preplasma, the heating of the preplasma and the atomic process can be modeled by a hot-spot model [12] in cooperation with a set of collisional-radiative rate equations, while the hydrodynamic expansion can be frozen during this process since the duration of the heating pulse and the x-ray laser gain is very short in comparison with the characteristic time of the evolution of the preplasma produced by the ns laser pulse.

We use self-similar model [18] to describe the evolution of the electron temperature and density of the preplasma. The peak temperature is set to be one-third of the ionization potential of the Na-like ion (for the Ne-like ion laser scheme) or that of the Cu-like ion (for the Ni-like ion laser scheme) of various target elements, in order to prepare a preplasma with one-third of the ions at the Ne-like or Ni-like stages, a reasonable assumption under steady state approximation. Of course we can use other values of peak electron temperature

to check its effect on the transient gain produced by the second pulse. For the preplasma, the relation between the electron temperature and the absorbed laser intensity is established by the thermal balance in a steady state ablation [19]. The mass ablation rate is also calculated under the same frame [20].

The hot-spot model [12] we used is a rather simple description of the short pulse laser energy deposited in a small plasma volume with uniform initial density and temperature. The absorption mechanism of the laser energy is inverse bremsstrahlung [21] only, thus it gives the lower limit of the absorbed laser energy. The dissipating channels of the deposited energy consist of the heating of electrons and ions, the excitation, and ionization energy of ions and the thermal conduction to the surrounding region with lower temperature. Other energy loss channels such as radiation and the adiabatic expansion are ignored in this model. The thermal conduction loss is described in a phenomenological way, and is proportional to the electron ion collision time and inversely proportional to the electron temperature gradient scale length [12]. This scale length actually defines to a large extent the cooling rate and is an adjustable variable in this work for studying its effect on the gain, as will be discussed in the following parts. We consider the effect of electron quiver energy in a strong laser field by using an expression of effective temperature that is the sum of the ponderomotive potential and the thermal temperature.

We limit our study only for the two $J=0$-1 lasing lines of Ne-like or Ni-like ions. The lasant ion stage is modeled with the ground state and four excited levels, i.e., the $2p^53s^{13}P_1$, $2p^53s^{11}P_1$, $2p^53p^{11}S_0$ and $2p^53d^{11}P_1$ levels for the Ne-like ion scheme or the $3d^94p^1(5/2,3/2)1$, $3d^94p^1(3/2,1/2)1$, $3d^94d^1(3/2,3/2)0$, and $3d^94f^1(3/2,5/2)1$ levels for the Ni-like ion scheme, since the reabsorption of the strong Ne-like $3d$-$2p$ or Ni-like $4f$-$3d$ transition in an optically thick plasma also contribute considerably to the population of the upper laser level, although the main populating channel is the monopole collisional excitation from the ground state. In this atomic model we include also the ground state of the next ionization stage of the lasant ion (the F-like stage in the Ne-like ion scheme or the Co-like stage in the Ni-like ion scheme). The above-mentioned six levels are the most important levels related to the $J=0$-1 laser. Some of the related atomic parameters are cited in the literature [5,16,22–26], and others are calculated by empirical formulas [27]. The opacity of resonant lines is measured by using escape factors that are calculated with the formulas shown in Ref. [28].

The self-similar model produces the density and temperature profiles of the preplasma, and then the hot-spot model and the rate equations for simplified level structure produce the gain coefficient profiles, which are postprocessed by a two-dimensional (2D) ray tracing model to integrate the laser gain along the x-ray laser propagation channel. This last model includes the refraction of x rays and the longitudinally pumping laser beam and the change of gain coefficients with positions in this channel. The nonlinear effect of the propagation of an intense short laser pulse in plasmas is also considered in the design.

III. TEST CALCULATIONS FOR X-RAY LASERS IN Ne-LIKE Ge AND Ni-LIKE Mo IONS

In order to check the validity of the above-described models, we first make calculations for the Ne-like Ge and Ni-like Mo x-ray laser systems and compare the results with the published work using sophisticated models [13–15]. In Ref. [13], the transient gain of the Ne-like Ge laser was calculated with a detailed model EHYBRID, which includes detailed hydrodynamics of the plasma and detailed atomic physics of the lasant ion (with 124 excited levels for the lasant ion stage and a simpler description of the other ion stages). In Refs. [14] and [15], the gains of the Ne-like Ge, Ti, and Ni-like Mo ion laser systems were calculated by assuming the same laser condition with LASNEX and XRASER codes.

We assume that a preplasma with one-third of the ions in the Ne-like Ge ground state and with an initial electron temperature of 350 eV and an electron density of $0.999n_c$ ($n_c = 10^{21}$ cm^{-3} is the critical electron density) is prepared before the arrival of the 1.05 μm 1 ps (full width at $1/e$ maximum intensity) Gaussian-shaped heating pulse peaking at 1 ps. These parameters are chosen in order to keep a preplasma condition similar to that shown in Ref. [13]. The level energies and transition probabilities used in the calculation are cited from Ref. [22].

We first conduct numerical experiments with different values of the peak intensity of the main heating pulse and with different values of the electron temperature gradient scale length, in order to discover a combination of suitable laser intensity and scale length that can produce a similar time profile of the electron temperature to that shown in Fig. 4 of Ref. [13]. We find that a peak intensity of 4.3 PW cm^{-2} and a scale length of 50 μm can produce a very similar time profile of electron temperature to that shown in Ref. [13]. The peak temperature is 1773 eV, and it falls to 1110 eV at 10 ps and to 850 eV at 20 ps in this work, while it peaks with 1750 eV and falls to 1050 eV at 10 ps and 870 eV at 20 ps as can be found in Fig. 4 of Ref. [13]. However, we notice a difference in laser intensity for producing this very similar temperature profile in this work and in Ref. [13]. The laser pulse profile used in Ref. [13] is a trapezium-shaped pulse with a peak intensity of 1 PW cm^{-2} that corresponds to a Gaussian pulse with a peak intensity of 1.7 PW cm^{-2} containing the same laser energy. So the laser intensity used in this work is 2.5 times larger. However, the EHYBRID code used in Ref. [13] may overestimate the energy absorption in collisionaly pumped laser by a factor of 2 [13,29]. Considering this modification, we find reasonable agreement in predicting the temperature with the simple hot-spot model and with the sophisticated code [13]. The remaining minor difference can be attributed to the fact that Ref. [13] considered the resonant absorption in addition to the inverse bremsstrahlung absorption. With the values of the laser intensity and the temperature scale length as mentioned, the time profile of the small signal gain of the Ne-like Ge ion $J=0$-1 laser is then calculated. The peak gain of the 19.6-nm laser is found to be 77 cm^{-1}, which is only half of that predicted in Ref. [13]. Some change in the escape factors for Ne-like Ge ion 3-2 resonant lines may cause some variation in the laser gain; however, it is found that this issue cannot account for the large difference observed for the peak gain. The difference in

peak gain might be attributed to the fact that our atomic model is too simple. However, we find that the gain value seems reasonable when we compare it with the work reported in Ref. [14].

The Ne-like Ti and Ge x-ray laser simulations were reported in Ref. [14]. The initial preplasma condition for the calculation in Ref. [14] is different from that assumed above. The first pulse was a 1.5 ns 1.05 μm laser pulse with an intensity of 1.2 TW cm^{-2}, while the second pulse was a triangular-shaped pulse with a 1-ps full width at half maximum and peak intensity of 1.2 PW cm^{-2}. If being fully absorbed, the first pulse can generate a preplasma with a peak temperature of about 350 or 250 eV based on the steady absorption approximation if the flux limit factor is assumed to be 1/30 or 1/20, respectively. However, it is found that this may overestimate the peak temperature when we examine the prepulse intensity and the preplasma temperature shown in Ref. [13]. Taking into account the difference in the pulse shape and laser energy of the nanosecond prepulses used in Refs. [13] and [14], we assume that the peak temperature of the preplasma is 200 eV in the following calculations for comparing the calculated gains with those shown in Ref. [14]. The assumption of the initial abundance of Ne-like ground state ions as stated in Sec. II becomes not so reasonable at this temperature for both Ne-like Ti and Ge ions. A temperature gradient scale length of about 15 μm is inferred from Fig. 2 of Ref. [14]. A laser intensity of 4.7 PW cm^{-2} for a 1-ps (full width at $1/e$ maximum intensity) Gaussian-shape pulse peaking at 1 ps is found to be able to heat the Ti plasma to a peak electron temperature of 1450 eV, a value given in Ref. [14]. Alternately, an intensity of 4.1 PW cm^{-2} is enough to generate the same peak temperature if the scale length is 30 μm. But the calculated laser gains are quite similar in the two cases. It suggests that the choice of temperature scale length in this range seems not so critical. The scale length of 15 μm is used in the following calculations. Comparing the calculated time profile of electron temperature with the data shown in Fig. 2 of Ref. [14], we find that the leading edge of this time profile agrees well with the data shown in Ref. [14], but the temperature decreasing rate is slower in this work, which might be attributed to the simplified consideration of the energy dissipating channels in the hot-spot model, as stated in Sec. II. The temperature peaks at 1.5 ps with a value of 1450 eV in this work, while the temperature peaked at 1.3 ps with a value of 1450 eV in Ref. [14]. For lack of accurate rate data for some transitions involved, we will not go into detail to compare the calculated gain for the Ne-like Ti system with Ref. [14]. We will, however, make calculations for the Ne-like Ge system again using the newly derived parameters.

The Ne-like Ge ion system is simulated again under the same conditions as the Ne-like Ti ion system, i.e., the preplasma density and temperature, the temperature gradient scale length, and the main pulse laser intensity. Rather good agreement in predicting the peak gain is found when we compare the calculated results with those given in Ref. [14]. The 19.6-nm laser gain peaks with 86 cm^{-1} at 3 ps, while the peak gain was predicted to be 54 cm^{-1} in Ref. [14]. Another feature is that there is an obvious delay for the peak gain with respect to the peak of the driving pulse. We find that this delay might originate from the opacity effect of the

resonant lines and the transient effect of the short pulse excitation process. The overestimation of laser gain in this work can be attributed mainly to the simplified level structure for the lasant ion. For comparison, calculations of the collisional-radiative rate equations including the first 30 excited levels of the Ne-like Ge ion are preformed and the resulting gain is only 85% of that obtained with the six-level system. The reason is that the populating and depopulating channels connecting a number of neighboring excited levels and the lasing levels are also important in high density plasmas. Similar calculations are also performed for the plasma with an electron density of 5×10^{20} cm^{-3} and a difference of 10% in the laser gain is found when comparing the six-level system with the much more complicated system involving the first 30 excited levels of the lasant ion. This suggests that the simple six-level system is more reasonable for a relatively low density plasma region.

The Ni-like Mo ion scheme is calculated under the same conditions as mentioned above, except that the electron density is assumed to be 8.5×10^{20} cm^{-3}, a value given in Ref. [15]. The related level energies and transition probabilities were calculated with the RELAC code [30]. The calculated plasma temperature peaks with 1450 eV at 1.5 ps, while it peaks with 1500 eV at 1.4 ps as shown in Ref. [15]. As in the case of the Ne-like Ti laser, we find again that the leading edge of the time profile of the temperature agrees well with the data shown in the Fig. 2 of Ref. [15], but the decreasing rate of temperature is slower in the present work. The peak gain of the 18.9 nm laser is 210 cm^{-1} and it is only about 54% of that predicted in Ref. [15]. We find that the preplasma temperature of 200 eV is so high that a considerable gain emerges even without the main heating pulse. The underestimation of the laser gain as compared with Ref. [15] might be attributed to the fact that the preplasma condition is not the same as that in the work reported in Ref. [15]. The ion temperature is 70 eV in the peak gain region as mentioned in Ref. [16]; however, the ion temperature is about 200 eV in the present calculation since the ion temperature and electron temperature are assumed to be of the same value in the preplasma. Taking into account the ion temperature dependence of the laser gain, we find that the modified laser gain (~ 355 cm^{-1}) is quite similar to that (387 cm^{-1}) predicted in Ref. [15]. However, the inaccuracy of the assumed abundance of Ni-like Mo ground state ions under the preplasma condition should be considered. If the preplasma temperature is assumed to be 100 eV, a value that makes the assumption of the abundance of Ni-like Mo ground state ions more reasonable as stated in Sec. II, the calculated gain of the 18.9-nm laser peaks with 550 cm^{-1} at 0.95 ps. Again the gain is overestimated and the extent of the overestimation is quite similar to that mentioned in the preceding paragraph for the Ne-like Ge ion laser. A similar argument can therefore be used to explain the overestimation of the laser gain.

The above-described test calculations and the comparisons with the results obtained by the two sophisticated models clearly show that the model presented in this work can predict very well the time history of the electron temperature and the timing of the laser gain as well, by choosing a reasonable temperature gradient scale length. This model may overestimate the necessary pumping laser intensity. The pre-

dicted laser intensity is 3.9 times the value predicted by the LASNEX and XRASER codes [14,15], while it is 2.5 times the value predicted by the EHYBRID code [13]. For the Ne-like Ge laser system driven under the above-mentioned conditions, the predicted gain is only about half of that calculated by EHYBRID code, but the predicted laser gain seems more similar to that calculated with the LASNEX and XRASER codes and the remaining small discrepancy can be explained by the incompleteness of the simple level structure for describing the lasant ions. The Ni-like Mo system has also been checked and the comparison with Ref. [15] shows that the calculated gain with the present model is reasonable. Based on the above analysis, this model is creditable and it can predict successfully the overall features of a transient gain laser system.

IV. DESIGN OF THE LONGITUDINALLY PUMPED Ni-LIKE Mo 18.9-nm X-RAY LASER

A. Calculations of the small-signal gain coefficient

The Ni-like $J = 0$-1 lasing line pair mentioned in Sec. II is for a Ni-like model ion of general purpose; however, the two strongest $J = 0$-1 lasing lines are $3d^9 4d^1(3/2,3/2)0 - 3d^9 4p^1(5/2,3/2)1$ (18.9 nm) and $3d^9 4d^1(3/2,3/2)0 - 3d^9 4p^1(3/2,3/2)1$ (19.7 nm) for the Ni-like Mo ion, and the two lines are therefore calculated with the model. As mentioned, the level energies and the related transition probabilities are calculated with the parametric potential code RELAC [30], only the energy of the upper laser level is shifted in the way mentioned in Ref. [15].

The calculation with YODA [31] for the monopole collisional excitation rate shows that the $3d^{10} - 3d^9 4d^1(3/2,3/2)0$ monopole collisional excitation transition of Ni-like Mo ion has a maximum rate of 4×10^{-10} cm^3/s when the electron temperature is in the range of 500–800 eV [5]. We therefore choose a peak temperature in this region in the design since a higher temperature is not necessary. For the transient gain scheme, a higher electron density produces a larger small-signal gain coefficient; however, we have to make a compromise between the high electron density (high gain) and long effective medium length since we are going to pump the preplasma longitudinally, and we also try to avoid using the very steep critical density surface. On the other hand, the principal advantage of the transient gain scheme will be lost if the density is too low. We therefore prefer the gain region of a moderate electron density. Figure 1 shows the 18.9-nm laser gain profiles calculated with several electron density values, i.e., 1×10^{20}, 1.5×10^{20}, and 2×10^{20} cm^{-3}. As shown the laser gain is very sensitive to the plasma density. Fortunately the gain at a density of 1.5×10^{20} cm^{-3} is large enough, and it is relatively easy in this density region to get a large scale length in a nanosecond pulse produced plasma so that the refraction issue might not be so serious as that at the critical density region. We will investigate only this density region in the following calculations.

The peak temperature of the preplasma is set to be 100 eV, which approximately equals 1/3 of the ionization potential of the Cu-like Mo ground state ion (303.9 eV [31]). For
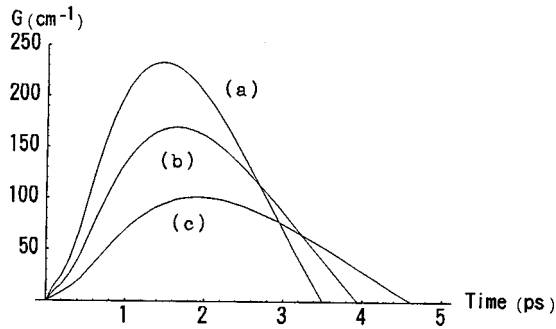
FIG. 1. The gain profiles of the 18.9-nm laser calculated with several density values. (a) 2×10^{20}, (b) 1.5×10^{20}, and (c) 1×10^{20} cm^{-3}.

a ns laser pulse at 1.05 μm, an intensity of ~ 0.2 TW/cm^2 is enough to produce such a preplasma. The evolution of the density and temperature of the preplasma is then calculated using the self-similar model. As discussed in the preceding section, the temperature gradient scale length determines the cooling rate, and it is a free variable in our calculation. We consider this issue at first since the cooling rate will determine the duration of the gain. Figure 2 shows the time profiles of the electron temperature and the gain of the Ni-like Mo ion 18.9 nm laser calculated with three possible values of the temperature gradient scale length, i.e., 10, 30, and 100 μm. The peak laser intensity is 3 PW/cm^2, the corresponding peak temperature ranges from 520 to 660 eV. The gain seems not so sensitive to the temperature gradient scale length in the range of 10 to 100 μm. The 10-μm scale length produces a slightly low gain and a slightly short duration of gain. A much smaller scale length seems impractical in the actual plasma since we are going to pump the 1.5×10^{20}-cm^{-3} density region longitudinally with a large F number focused laser beam with a waist size of about 100 μm. We therefore use the scale length of 30 μm in the following calculations. The related timing of the pumping laser pulse, the electron temperature profile, and the gain profile of the two x-ray lasing lines (18.9 and 19.7 nm) are shown in Fig.
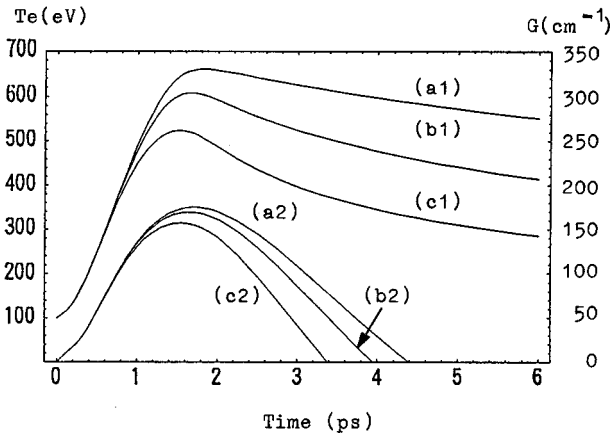

FIG. 2. The time profiles of the electron temperature ($a1,b1,c1$) and the gain ($a2,b2,c2$) of the Ni-like Mo ion 18.9-nm laser calculated with three possible values of the temperature gradient scale length, i.e., (a) 100, (b) 30, and (c) 10 μm. The peak laser intensity is 3 PW/cm^2.
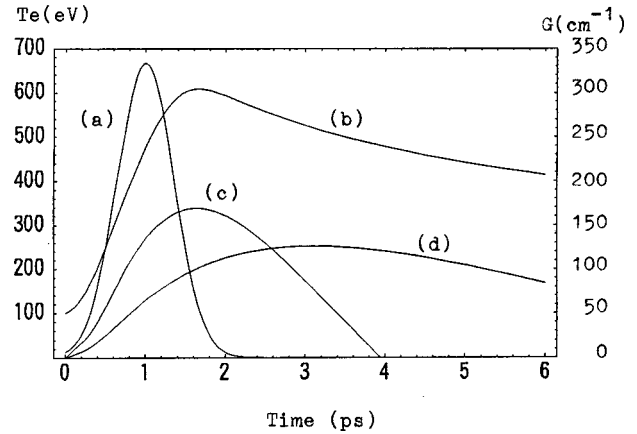

FIG. 3. The related timing of the pumping laser pulse (a), the electron temperature profile, (b), and the gain profiles of the 18.9-nm (c) and 19.7-nm (d) x-ray lasing lines.

3. The gain of the 18.9- and 19.7-nm laser peaks with 170 and 126 cm^{-1} at 1.6 and 3.1 ps, respectively. By using the formulas given in Ref. [28], the escape factors are calculated to be 0.0032 ($f1$), 0.0163 ($f2$), and 0.00043 ($f3$) for the three 4-3 resonant lines originating from the lower laser levels of the 18.9- and 19.7-nm lasers, and the $4f$ level, respectively. The results shown in Figs. 1–3 were computed with these values. However, these escape factor values were derived for a static plasma case and the opacity of resonant lines can be reduced in the expanding plasma with a large velocity gradient. In order not to introduce further error in gain calculations due to the uncertainty in the plasma velocity gradient, the escape factors are varied phenomenologically over several orders of magnitude and the resulting change in laser gains are then investigated. It is found that, if the escape factor of the resonant transition originating from the $4f$ level is kept as $f3$ and the escape factors of the resonant lines originating from the lower laser levels are increased by two orders of magnitude from the nominal values, i.e., $f1$ and $f2$, the peak gain of the 18.9-nm laser is only increased by 10%, while no change is observed for the laser gain if the escape factors are reduced by two orders of magnitude. This suggests that the results (as shown in Figs. 1–3 obtained with the nominal values ($f1$ and $f2$) are the lower limit of the laser gain determined by the opacity of the emptying transitions of the lower laser levels. On the other hand, if the escape factors of the resonant transitions originating from the lower laser levels are kept as the nominal values ($f1$ and $f2$) and the escape factor of the resonant line originating from the $4f$ level is increased by two orders of magnitude from the nominal value $f3$, the peak gain of the 18.9-nm laser is only reduced by 12%, while no change is observed for the laser gain if the escape factor is reduced by two orders of magnitude. This suggests that the nominal value $f3$ (used in the calculations for Figs. 1–3) accounts for the upper limit of the possible opacity effect of the $4f$-$3d$ transition on the laser gain. Actually the escape factors for the three resonant lines change simultaneously in the expanding plasma with a large velocity gradient. Shown in Fig. 4 is a comparison of the gain profiles of the 18.9-nm laser calculated with four sets of values for the escape factors. Curves a and b, which are almost overlapping are obtained
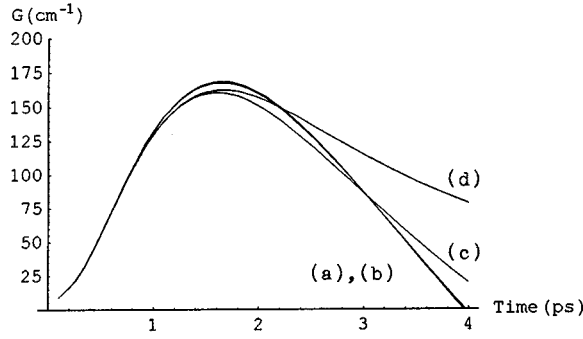
FIG. 4. The change of the 18.9-nm laser gain profile if the escape factors of the resonant lines are changed. Curves *a* and *b*, which are almost overlapping are obtained with the norminal escape factors ($f1$, $f2$, and $f3$) and $10 \times f1$, $10 \times f2$, and $10 \times f3$, respectively. Curve *c* is obtained with $100 \times f1$, $f2 = 1$, and $100 \times f3$, and curve *d* is obtained with $f1 = f2 = 1, f3 = 0.1$, respectively.

with the nominal escape factors ($f1$, $f2$, and $f3$) and $10 \times f1$, $10 \times f2$, and $10 \times f3$, respectively. Curve *c* is obtained with $100 \times f1$, $f2 = 1$ and $100 \times f3$, and curve *d* is obtained with $f1 = f2 = 1, f3 = 0.1$, respectively. It is found that there is only a little change in the peak gain in all four cases. The above investigation of the opacity effect of the Ni-like Mo resonant lines on the laser gain shows that the peak gain seems not so sensitive to the opacity as the duration of the laser gain does.

The peak gain as a function of the intensity of the main heating pulse is shown in Fig. 5. One can find that the gain is quite stable if the pumping intensity is higher than ~ 2 PW/cm^2. The operating laser intensity is therefore chosen in this range in the design.

B. Propagation of the pumping beam in the Mo plasmas

The schematic of the proposed pumping geometry is shown in Fig. 6. The calculations in the preceding section show that the pumping beam has to propagate in the plasmas over a distance of several millimeters to make the x-ray laser amplification saturated.

The propagation of an intense laser pulse in plasmas is affected by linear effects such as the Rayleigh diffraction and the plasma density gradient induced refraction and by the nonlinear response of the plasma to the intense laser pulse,
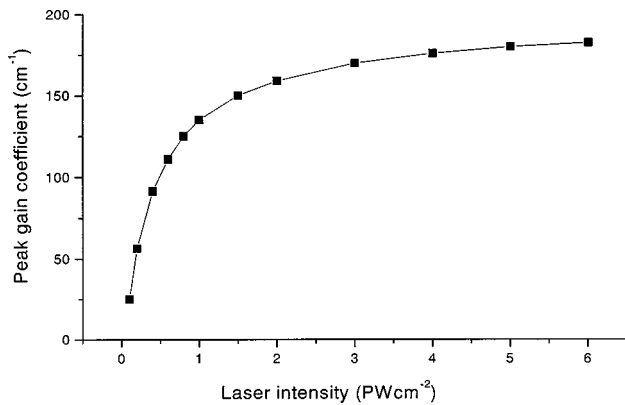

FIG. 5. The peak gain as a function of the intensity of the main heating pulse.
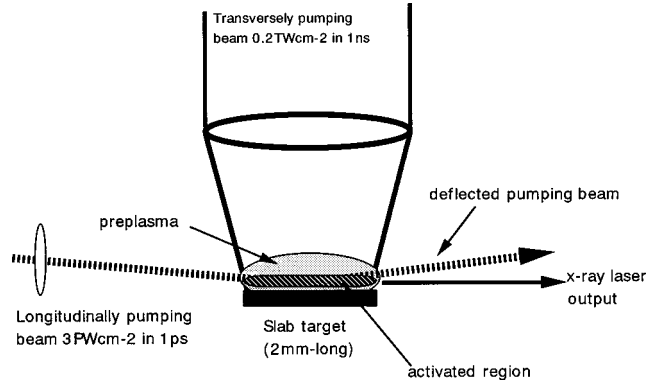

FIG. 6. The schematic of the proposed pumping geometry.

such as the ionization-induced refraction, relativistic effects, ponderomotive effects, plasma wave effects, and instabilities. We first analyze these nonlinear effects. In the above-described calculations, the electron density is assumed to be unchanged during the interaction of the main pulse with the preplasma. This assumption is now examined by investigating the possibility of collisional and field-induced ionizations. The collisional ionization is already included in our model and the calculated results show that the ionization is negligible during the picosecond-long interaction time between the laser and the plasma. The ionization potential of Ni-like Mo ground state ions is 544 eV [30], and the maximum electron quiver energy induced by the employed laser field is about 300 eV, then the Keldysh parameter $\gamma \sim 1$. The optical-field-ionization process is therefore an interplay between multiphoton processes and tunneling. For simplicity, the well-known Ammosov-Delone-Krainov (ADK) formula [32] for tunneling ionization is used to calculate the optical-field-ionization rate of the Ni-like Mo ion subjected to the laser field. The calculated photoionization rate is so small that the ionization during the laser pulse can also be ignored. Of course, the photoionization of the very weakly ionized Mo ions will have a considerable rate if their ionization potential is lower than 100 eV. However, as assumed, the Ni-like Mo ions dominate in the preplasma, the abundance of the very weakly ionized ions is relatively very low. It suggests that the ionization-induced refraction is not important in the parameter space where the designed x-ray laser operates. The propagation of the pumping laser beam in the Ni-like Mo plasmas can therefore be approximately regarded as the propagation in a fully ionized plasma environment.

The general expression for the refractive index for a large amplitude electromagnetic wave in a fully ionized plasma is given by

$$n(r) = \left(1 - \frac{\omega_p^2}{\omega_l^2} \frac{n_e(r)}{n_{e0}\gamma(r)} \right)^{1/2}, \qquad (1)$$

where $n_e(r)$ is the local electron density, n_{e0} is the ambient plasma electron density, $\gamma(r)$ is the relativistic factor associated with the plasma electrons, and ω_p and ω_l are electron plasma frequency and laser frequency, respectively. The relativistic factor reads as [33]

$$\gamma \doteq (1 + a^2/2)^{1/2}, \qquad (2)$$

where a is the laser strength parameter, $a^2 \propto I$, and I is the laser intensity. For the laser intensity $\sim 10^{15}$ W/cm^2 used in this design, $a^2 \ll 1$, so it is in the mildly relativistic limit [33]. The relativistic self-focusing is possible only if the laser power is higher than the critical power and the pulse length is longer than the plasma wavelength. The critical power for guiding, including the effects of relativistic self-focusing and pondermotive self-channeling, is [33,34]

$$P_c = 16.2(\omega_l^2/\omega_p^2)(\text{GW}).   (3)$$

For the Ni-like Mo plasmas, the electron density is 1.5×10^{20} cm^{-3}, then $P_c = 108$ GW, and the plasma wavelength λ_p is 2.7 μm. The peak laser intensity is 3×10^{15} W/cm^2 and the focus size is 100 μm, so the maximum laser power P is about 235 GW($> P_c$), and the pulse length ($L = c \times \tau$) is 300 μm ($\geq \lambda_p$), the relativistic self-focusing is therefore possible in the present case. The spot size as a function of the propagation distance is approximately given by [33]

$$r_s^2/r_0^2 = 1 + (1 - P/P_c)z^2/z_R^2,   (4)$$

where r_0 is the minimum spot size in vacuum, and z_R is the vacuum Rayleigh length. As mentioned, the spot size r_0 assumed in this design is 100 μm and it corresponds to a Rayleigh length of about 3 cm for the 1.05-μm laser. The spot size is decreased by only 0.3% after propagating for 2 mm. Actually, the laser power will be reduced dramatically during the propagation due to the strong inverse bremsstrahlung absorption in the plasma. In this case, the change of spot size is even more negligible. This long Rayleigh length also assumes that the vacuum diffraction is not considerable over the short propagation distance of several mm.

A long laser pulse ($L > \lambda_p$) that is guided by relativistic self-focusing is subject to severe self-modulation due to the plasma wave excited by the ponderomotive force associated with the finite rise of the laser pulse; the modulation can strongly affect the focusing properties of the pulse body, and self-modulation instability will grow as well in this situation. The interplay of self-focusing and self-modulation can be well described by the wave equation (116) shown in Ref. [33]. The square of the ratio of laser pulse rise time L_{rise} to plasma wavelength λ_p is an important factor for checking whether a density wake can be excited and affects the focusing of the pulse body [33]. In the present case, the laser pulse is a gradually turned-on Gaussian shape pulse, so $(L_{\text{rise}}/\lambda_p)^2 \gg 1$, the initial density wake vanishes and the focusing is determined solely by the relativistic self-focusing. Calculations show that the modulation is growing as a function of both the propagation distance and the distance behind the pulse front [33]. If there is any modulation in the present case, the actual effect can be ignored because the propagation distance is considerably shorter than one Rayleigh length in this design. The above analysis has shown that there is some very weak self-focusing under the experimental conditions we designed. However, recently reported experiment [35] on the propagation of a 600-fs pulse in plasmas suggests that the energy threshold for the relativistic self-focusing is considerably higher than that predicted by the linear theory, which we used in the preceding analysis. Con-
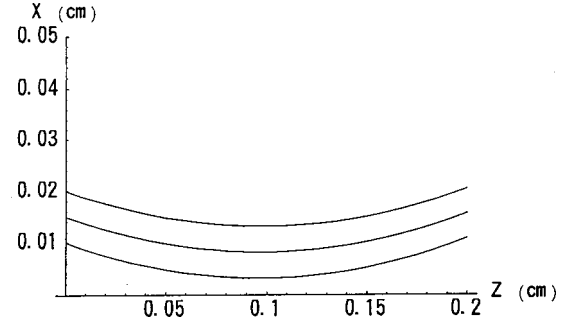

FIG. 7. The trace of the pumping beam in the preplasma with a mean density of 1.5×10^{20} cm^{-3} and a scale length of 1.25 mm.

sequently, the nonlinear response of the plasma to the propagation of the main heating pulse in the Ni-like Mo plasma can be ignored in the parameter space where the x-ray laser operates. Therefore the most important problem that the pulse will encounter during the propagation is the refraction induced by the density gradient in the expanding plasma.

Because of the density gradient induced refraction, the traces of the optical laser and the x rays in plasmas are quite different since the corresponding critical densities differ considerably. For the preplasma produced by a laser intensity of 0.2 TW/cm^2 with a duration of 1 ns, the density gradient scale length for the 1.5×10^{20}-cm^{-3} region is calculated to be about 50 μm at 1 ns and 1.25 mm at 3 ns. The density gradient at 1 ns is too large for optical rays to propagate over a reasonable distance in the plasma. While a scale length of 1.25 mm is good for the 1.05-μm optical ray to propagate over several mm before refracting out from the region of interest. However, the electron temperature of the preplasma will fall to about 30% of the peak temperature (about 30 eV in this specific case), and the abundance of Ni-like ions will also decrease consequently. Fortunately the well-developed prepulse technique can be used here to solve this problem. We can use two pulses to produce a preplasma before the arrival of the main heating pulse. At present the simple self-similar model cannot account for the double-pulse produced plasma; however, the assumption that the density profile is mainly defined by the first pulse is valid if the delay of the second pulse is not too short, i.e., several ns in the present case. We can still use the above-derived density scale length in the calculation of the propagation, by assuming that we have another ns pulse to reheat slightly the plasma to 100 eV
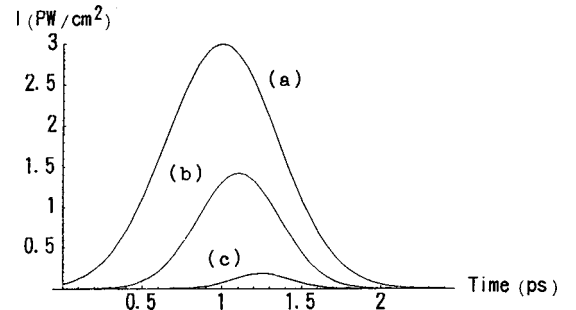

FIG. 8. The change of the time profile of the driving laser pulse at three positions along the plasma column. (a) $z = 0$, (b) $z = 1$ mm, and (c) $z = 2$ mm.
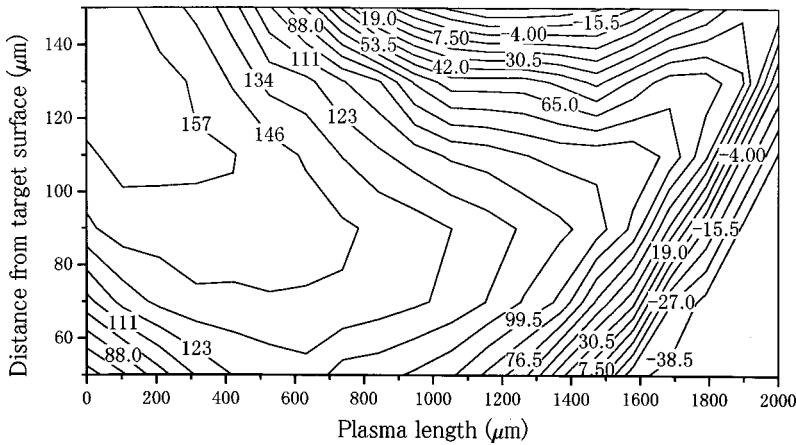
FIG. 9. The 2D distribution of the gain coefficient of the 18.9-nm laser at 1.8 ps in the plasma column.

before the main heating pulse arrives, so that the abundance of the Ni-like ion is roughly the same as that we used to calculate the gain, as mentioned above.

The trace of the pumping beam in the preplasma with a mean density of 1.5×10^{20} cm^{-3} and a scale length of 1.25 mm is shown in Fig. 7; only the refraction effect is considered in the calculation. In Fig. 7, the 1.05-μm optical rays enter the plasma from the left, and the Z axis measures along the propagation direction, while the X axis measures the distance away from the target surface. In order to get long propagation distance, the beam enters the plasma at an incidence angle of 0.14 rad measured from the target surface. Since we are going to use a large F number focused beam with a waist size of 100 μm in the experiment, where the Rayleigh range is larger than the effective propagation distance defined by the refraction effect, a collimated beam is used in the present calculations. The change of the pulse intensity and duration due to the inverse bremmsstrahlung absorption at three positions along the plasma column is shown in Fig. 8. One finds that most of the laser energy is deposited in the 2-mm plasma column. Assuming that the intensity distribution in the driving laser beam profile is Gaussian like and the waist size is 100 μm (full width at half-maximum), the 2D distribution of the gain coefficient of the 18.9-nm laser in the plasma column is then calculated and the calculated laser gain at 1.8 ps is shown in Fig. 9. We integrate the gain along the propagation direction and obtain the spatial distribution of the GL value for different plasma lengths. The time-resolved GL product of the 18.9-nm laser for a 2-mm-long plasma is shown in Fig. 10. In the calculations, we simply compute the integrated GL value without considering the effect caused by the saturation of amplification. One can see that the gain saturation can be attained in a ~60-μm-wide region and the duration is about 1 ps. Only about 235 mJ laser energy at 1 ps duration is enough to produce the necessary intensity of 3 PW/cm^2 if the beam is focused down to a 100-μm spot. According to the calculated results, a saturated Ni-like Mo laser at 18.9 nm can be implemented by using a 1.05-μm driving laser with only several hundred mJ energy, including the energy of the 1-ns-duration pulse for producing the preplasma and the energy of the 1-ps-duration main heating pulse.

The results look very promising. However, the gain coefficient was calculated with a set of simplified models in this work. In regard to the models we used in this work, the

hydrodynamic physics model for describing the preplasma is not of critical importance as long as the large scale length plasma with a mean density of 1.5×10^{20} cm^{-3} can be produced, which is not a big issue for the ns laser plasma interaction. The preparation of Ni-like ions in the ground state is also straightforward by a steady state laser ablation process. The energy deposition of the short pulse and the plasma heating were considered by the simple hot-spot model in this work, and the validity of this solution was verified in Sec. III. Therefore the most important source of possible error in our calculation might be the incomplete and simplified atomic model (the six-level model) and the inaccuracy of the atomic parameters we used. The validity of the six-level model was verified for the Ne-like Ge ion scheme and the possible error is also estimated by comparing the results with those calculated with a complicated level system. The atomic physics for the Ni-like ion is much more complicated since more levels are involved. However, we notice that a similar simplified level structure was used to predict successfully the lasing in the Ni-like Eu ion [36]. Therefore we believe the simplified atomic model can produce reasonable predictions. The level energies we used were calculated with the RELAC code [30] and were checked with some other calculations [5,16,37]. The dipole transition probabilities were calculated with the RELAC code also. The most important parameter involved in this work is the monopole collisional excitation
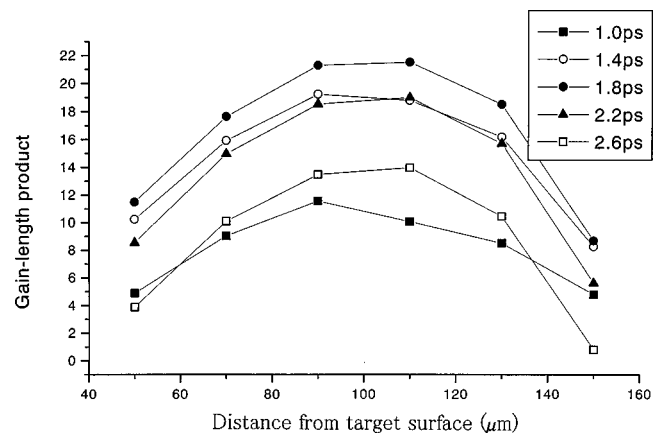

FIG. 10. The time-resolved spatial distribution of the GL values of the 18.9-nm laser for a 2-mm-long plasma at several moments (1.0, 1.4, 1.8, 2.2, and 2.6 ps).

rates, which were cited from Ref. [5], and they were calculated by the relativistic distorted wave code YODA [31], which has been widely used [5].

V. CONCLUSIONS

We have reexamined the transient gain scheme in this paper and have developed this scheme for designing a compact and highly efficient Ni-like Mo ion soft-x-ray laser. Model calculations showed that a saturated amplification of soft-x-rays at 18.9 nm can be realized by using only several hundred mJ energy from a 1.05-μm driving laser, including the energy of the 1-ns-duration pulse for producing the preplasma and the energy of the 1-ps-duration main heating pulse. We have also proposed a longitudinally pumping geometry for the high transient gain x-ray laser, this geometry can improve the pumping efficiency and overcome some limitations of the present transient gain laser by automatically traveling wave pumping and by sampling directly the desired gain region of a suitable density.

The models presented in this paper can be used to design a shorter wavelength Ni-like ion laser with a heavier target element. However, for shorter wavelength lasers, the operating density should be much higher; a pumping laser of shorter wavelength is then desired for producing higher critical density, which can also improve the propagation of the longitudinally pumping laser beam. However, at higher laser intensity and higher plasma density, the propagation of the pumping beam in the plasma becomes more complicated. The nonlinear response of the plasma to the laser pulse has to be taken into account to determine the optical laser traces in the plasma and the effective medium length responsible for the accumulation of soft-x-ray amplifications.

ACKNOWLEDGMENTS

[1] For recent reviews in this field, please see *X-ray Lasers 1996*, Proceedings of the 5th International Conference on X-ray Lasers, edited by S. Svanberg and C.-G. Wahstrom, IOP Conf. Proc. No. 151 (Institute of Physics, Bristol, 1996).

[2] J. Zhang, A. G. MacPhee, J. Nilsen, J. Lin, T. W. Barbee, Jr., C. Danson, M. H. Key, C. L. S. Lewis, D. Neely, R. M. N. O'Rourke, G. J. Pert, R. Smith, G. J. Tallents, J. S. Wark, and E. Wolfrum, Phys. Rev. Lett. **78**, 3856 (1997).

[3] J. Zhang, A. G. MacPhee, J. Lin, E. Wolfrum, R. Smith, C. Danson, M. H. Key, C. L. S. Lewis, D. Neely, J. Nilsen, G. J. Pert, G. J. Tallents, and J. S. Wark, Science **276**, 1097 (1997).

[4] P. V. Nickles, V. N. Shlyaptsev, M. Kalachnikov, M. Schnurer, I. Will, and W. Sander, Phys. Rev. Lett. **78**, 2748 (1997).

[5] H. Daido, S. Ninomiya, T. Imani, Y. Okaichi, M. Takagi, R. Kodama, H. Takabe, Y. Kato, F. Koike, J. Nilsen, and K. Murai, Int. J. Mod. Phys. B **11**, 945 (1997).

[6] P. Jaegle, A. Carillon, P. Dhez, P. Goedtkindt, G. Jamelot, A. Klisnick, B. Rus, Ph. Zeitoun, S. Jacquemot, D. Mazataud, A. Mens, and J. P. Chauvineau, in *X-ray Lasers 1994*, Proceedings of the 4th International Colloquium on X-ray Lasers, edited by D. Eder and D. Matthews, AIP Conf. Proc. No. 332 (AIP, New York, 1994), p. 25.

[7] A. Carillon, H. Z. Chen, P. Dhez, L. Dwivedi, J. Jacoby, P. Jaegle, G. Jamelot, J. Zhang, M. H. Key, A. Kidd, A. Kilsnick, R. Kodama, J. Krishnan, C. L. S. Lewis, D. Neely, P. Norreys, D. O'Neill, G. J. Pert, S. A. Ramsden, J. P. Raucourt, G. J. Tallents, and J. Uhomoibhi, Phys. Rev. Lett. **68**, 2917 (1992); J. Zhang, P. J. Warwick, E. Wolfrum, M. H. Key, C. Danson, A. Demir, S. Healy, D. H. Kalantar, N. S. Kim, C. L. S. Lewis, J. Lin, A. G. MacPhee, D. Neely, J. Nilsen, G. J. Pert, R. Smith, G. J. Tallents, and J. S. Wark, Phys. Rev. A **54**, R4653 (1996).

[8] J. A. Koch, B. J. MacGowan, L. B. DaSilva, D. L. Matthews, J. H. Underwood, P. J. Batson, and S. Mrowka, Phys. Rev. Lett. **68**, 3291 (1992).

[9] L. B. DaSilva, B. J. MacGowan, S. Mrowka, J. A. Koch, R. A. London, D. L. Matthews, and J. H. Underwood, Opt. Lett. **18**, 1174 (1993).

[10] Yu. V. Afanas'ev and V. N. Shlyaptsev, J. Quantum Electron. **19**, 1606 (1989); V. N. Shlyaptsev, P. V. Nickles, T. Schlegel, M. P. Kalashnikov, and A. L. Osterheld, Proc. SPIE **2012**, 111 (1993).

[11] N. H. Burnett and P. B. Corkum, J. Opt. Soc. Am. B **6**, 1195 (1989); Y. Nagata, K. Midorikawa, S. Kubodera, N. Obara, H. Tashiro, and K. Toyoda, Phys. Rev. Lett. **71**, 3774 (1993); B. E. Lemoff, G. Y. Yin, C. L. Gordon III, C. P. J. Barty, and S. E. Harris, *ibid.* **74**, 1574 (1995); J. Zhang, M. H. Key, P. A. Norreys, G. J. Tallents, A. Behjat, C. Danson, A. Demir, L. Dwivedi, M. Holden, P. B. Holden, C. L. S. Lewis, A. G. MacPhee, D. Neely, G. J. Pert, S. A. Ramsden, S. J. Rose, Y. F. Shao, O. Thomas, F. Walsh, and Y. L. You, *ibid.* **74**, 1335 (1995); D. V. Korobkin, C. H. Nam, S. Suckewer, and A. Goltsov, *ibid.* **77**, 5206 (1996).

[12] K. G. Whitney, A. Dasgupta, and P. E. Pulsifer, Phys. Rev. E **50**, 468 (1994).

[13] S. B. Healy, K. A. Janulewicz, J. A. Plowes, and G. J. Pert, Opt. Commun. **132**, 442 (1996).

[14] J. Nilsen, Phys. Rev. A **55**, 3271 (1997).

[15] J. Nilsen, J. Opt. Soc. Am. B **14**, 1511 (1997).

[16] P. L. Hagelstein, Proc. SPIE **1627**, 340 (1992).

[17] S. Basu, P. L. Hagelstein, J. G. Goodberlet, M. H. Muendel, and S. Kaushik, Appl. Phys. B: Photophys. Laser Chem. **57**, 303 (1993).

[18] A. V. Farnworth, Jr., M. M. Widner, M. J. Clauser, P. J. McDaniel, and K. E. Lonngren, Phys. Fluids **22**, 859 (1979); A. V. Farnworth, Jr., *ibid.* **23**, 1496 (1980).

[19] C. E. Max, in *Laser Plasma Interaction*, edited by R. Balian

and J.C. Adam (North-Holland, Amsterdam, 1982), p. 305.

[20] R. Fabbro, E. Fabre, F. Amiranoff, C. Garban-Labaune, J. Virmont, M. Weinfeld, and C. E. Max, Phys. Rev. A **26**, 2289 (1982).

[21] T. W. Johnston and J. M. Dawson, Phys. Fluids **16**, 722 (1973).

[22] M. Cornille, J. Duban, and S. Jacqucmot, At. Data Nucl. Data Tables **58**, 1 (1994).

[23] J. Nilsen, Opt. Lett. **15**, 798 (1990).

[24] M. Klapisch, J. L. Schwob, M. Finkenthal, B. S. Fraenkel, S. Egert, and A. Bar-Shalom, Phys. Rev. Lett. **41**, 403 (1978).

[25] J. Sugar, J. Reader, and W. L. Rowan, Phys. Rev. A **51**, 835 (1995).

[26] K. B. Fournier, W. H. Goldstein, M. May, and M. Finkenthal, Phys. Rev. A **53**, 709 (1996); K. B. Fournier, W. H. Goldstein, M. May, M. Finkenthal, and J. L. Terry, *ibid.* **53**, 3110 (1996).

[27] M. Itoh, T. Yabe, and S. Kiyokawa, Phys. Rev. A **35**, 233 (1987).

[28] R. C. Elton, *X-ray Lasers* (Academic, San Diego, 1990), p. 39.

[29] P. B. Holden, S. B. Healy, M. T. M. Lightbody, G. J. Pert, J. A. Plowes, A. E. Kingston, E. Robertson, C. L. S. Lewis, and D. Neeley, J. Phys. B **27**, 341 (1994).

[30] K. B. Fournier (private communications).

[31] P. L. Hagelstein, Phys. Rev. A **34**, 874 (1986); P. L. Hagelstein and S. Dalhed, *ibid.* **37**, 1357 (1988).

[32] M. V. Ammosov, N. B. Delone, and V. P. Krainov, Zh. Éksp. Teor. Fiz. **91**, 2008 (1986) [Sov. Phys. JETP **64**, 1191 (1986)].

[33] E. Esarey, P. Sprangle, J. Krall, and A. Tingm, IEEE J. Quantum Electron. **33**, 1879 (1997).

[34] G. Z. Sun, E. Ott, Y. C. Lee, and P. Guzdar, Phys. Fluids **30**, 526 (1987).

[35] P. E. Young and P. R. Bolton, Phys. Rev. Lett. **77**, 4556 (1996).

[36] S. Maxon, P. Hagelstein, J. Scotfield, and Y. Lee, J. Appl. Phys. **59**, 293 (1986).

[37] J. F. Wyart, Phys. Scr. **36**, 234 (1987).